

# Lattice QCD and High Baryon Density State

Keitaro Nagata<sup>1</sup>, Atsushi Nakamura<sup>1</sup>, Shinji Motoki<sup>1</sup>,  
Yoshiyuki Nakagawa<sup>2</sup> and Takuya Saito<sup>3</sup>

<sup>1</sup> Research Institute for Information Science and Education, Hiroshima University,  
Higashi-Hiroshima 739-8527 JAPAN

<sup>2</sup> Graduate School of Science and Technology, Niigata University,  
Niigata 950-2181, Japan

<sup>3</sup> Integrated Information Center, Kochi University, Kochi, 780-8520, Japan

November 13, 2018

We report our recent studies on the finite density QCD obtained from lattice QCD simulation with clover-improved Wilson fermions of two flavor and RG-improved gauge action. We approach the subject from two paths, i.e., the imaginary and real chemical potentials.

## 1 Introduction

QCD at finite temperature and density has been one of the most attracting subjects in physics. Many phenomenological models predict that the QCD phase diagram has a very rich structure, and thoroughgoing analyses of heavy ion data show that we are sweeping finite temperature and density regions. See Ref. [1].

First-principle calculations based on QCD are now highly called. If such calculations would be at our hand, their outcomes are also very valuable for many research fields: high energy heavy ion collisions, the high density interior of neutron stars and the last stages of the star evolution. Needless to say, the inside of nucleus is also a baryon rich environment, and lots of contributions to nuclear physics could be expected.

Unfortunately, the first principle lattice QCD simulation suffers from the sign problem. Nevertheless, there have been many progresses such as the reweighting method, the imaginary chemical potential and the canonical

formulation; now some light is shed on the QCD phase diagram. For reviews, see e.g. [2, 3].

Here, we report our recent trials to promote the finite density lattice QCD. It contains two results [4, 5]: the determination of the phase boundary of the deconfinement transition based on the imaginary chemical potential approach and a reduction formula for the Wilson fermion determinant.

## 2 Imaginary Chemical Potential Approach

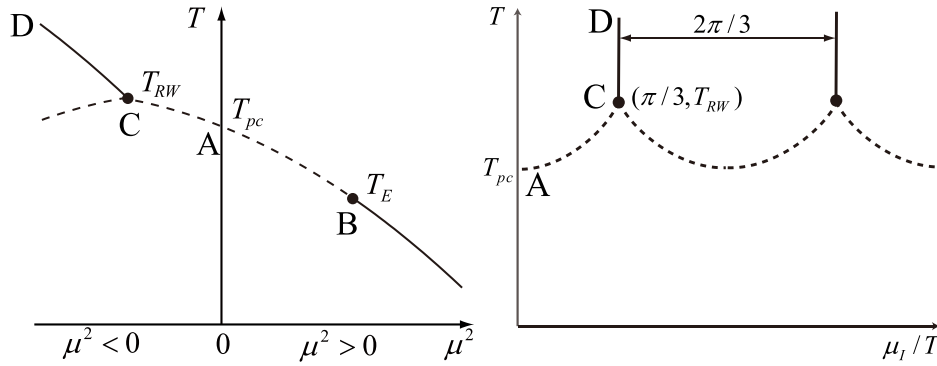


Figure 1: Schematic figures for the  $N_f = 2$  QCD phase diagram in the  $(\mu^2, T)$  plane (left) and  $(\mu_I/T, T)$  plane (right). A : Pseudo-critical point at  $\mu = 0$ . B : Critical endpoint. C : Roberge-Weiss endpoint. AB : Pseudo-critical line. AC : Extension of the line AB into the imaginary chemical potential plane. CD : Roberge-Weiss phase transition line  $\mu_I/T = \pi/3$ . In the right panel, larger  $\mu_I/T$  region of the phase diagram is obtained from the RW periodicity.

The QCD with an imaginary chemical potential is free from the sign problem. Using a relation

$$(\det \Delta(\mu))^* = \det \Delta(\mu), \quad (\mu = \mu_R + i\mu_I), \quad (1)$$

it is straightforward to prove that  $\det \Delta(\mu)$  is real for  $\mu = i\mu_I$ . A partition function and its free-energy are analytic within one phase even if chemical potential is extended to complex, which is true until the occurrence of a phase transition. This validates the imaginary chemical potential approach for the study of the QCD phase diagram. In addition, the QCD phase diagram in the imaginary chemical potential regions have a unique feature called the Roberge-Weiss periodicity [6], see Fig. 1. There have been several studies in staggered fermions [7–16] and standard Wilson fermions [17].

We employ a clover-improved Wilson fermion action of two-flavors and a renormalization-group improved gauge action. The clover-improved Wilson fermion action is given by

$$\begin{aligned} \Delta(x, y) &= \delta_{x, x'} - \kappa \sum_{i=1}^3 \left[ (1 - \gamma_i) U_i(x) \delta_{x', x+\hat{i}} + (1 + \gamma_i) U_i^\dagger(x') \delta_{x', x-\hat{i}} \right] \\ &\quad - \kappa \left[ e^{+\mu} (1 - \gamma_4) U_4(x) \delta_{x', x+\hat{4}} + e^{-\mu} (1 + \gamma_4) U_4^\dagger(x') \delta_{x', x-\hat{4}} \right] - \kappa C_{SW} \delta_{x, x'} \sum_{\mu \leq \nu} \sigma_{\mu\nu} F_{\mu\nu}. \end{aligned}$$

Here  $\mu$  is the quark chemical potential in lattice unit, which is introduced to the temporal part of link variables.

In order to scan the phase diagram, simulations were done for more than 150 points on the  $(\mu_I, \beta)$  plane in the domain  $0 \leq \mu_I \leq 0.28800$  and  $1.79 \leq \beta \leq 2.0$ . All the simulations were performed on a  $N_s^3 \times N_t = 8^3 \times 4$  lattice. The RW phase transition line in the present setup is given by  $\mu_I = \pi/12 \sim 0.2618$ . The value of the hopping parameter  $\kappa$  were determined for each value of  $\beta$  according to a line of the constant physics with  $m_{PS}/m_V = 0.8$  obtained in Ref. [18].

Scatter plots of the Polyakov loop in the complex plane are shown in Fig. 2, where we choose two typical cases  $\beta = 1.80$  for the hadronic phase and  $\beta = 1.95$  for the QGP phase. At low temperatures, the Polyakov loop is small in magnitude for any  $\mu_I$  and continuously changes in a clockwise direction as increasing  $\mu_I$ . On the other hand, at high temperatures, the Polyakov loop grows to  $0.2 \sim 0.3$ . It stays at the real axis for  $\mu_I < \pi/12$  and jumps to the left-lower side at  $\mu_I = \pi/12$ . The difference of the Polyakov loop modulus between high and low temperatures shows the deconfinement crossover, which is the curve AC in Fig. 1. The observed jump of the Polyakov loop at  $\mu_I = \pi/12$  is the Roberge-Weiss phase transition, which is the line CD. Thus, the phase structure in  $\mu^2 < 0$  regions of the QCD phase diagram can be determined by observing the behavior of the Polyakov loop. The properties of the phase transitions and RW endpoint are obtained from the susceptibility of the Polyakov loop. We obtain the location of the RW endpoint  $\beta = 1.927(5)$ , which corresponds to  $T/T_{pc} \sim 1.15$ .

Critical values of  $\beta$  for the deconfinement transition are obtained from the susceptibility of the Polyakov loop modulus for each  $\mu_I$ . Using the data for the critical values of  $\beta$ , we can determine the pseudo-critical line. Obtained pseudo-critical line is analytically continued to  $\mu^2 > 0$  region. The results are shown in Fig. 3, where we employ physical unit ( $\mu = \hat{\mu}a$ ). The curvature at  $\hat{\mu}/T_{pc} = 0$  of a power series of  $(\hat{\mu}/\pi T_{pc})^2$  is  $t_2 = \pi^2 d_2 = 0.38(12)$ . The present results are slightly smaller than other studies, see e.g. Ref. [19]

### 3 Reduction Formula for Wilson Fermions

In the lattice QCD simulations with finite chemical potential  $\mu$ , often we must handle the fermion determinant  $\det \Delta(\mu)$ , directly. For example, the reweighting method requires a ratio of two determinants,  $\frac{\det \Delta(\mu')}{\det \Delta(\mu)}$ ; The density of state method needs the phase information[20]; The canonical formulation needs the Fourier transformation

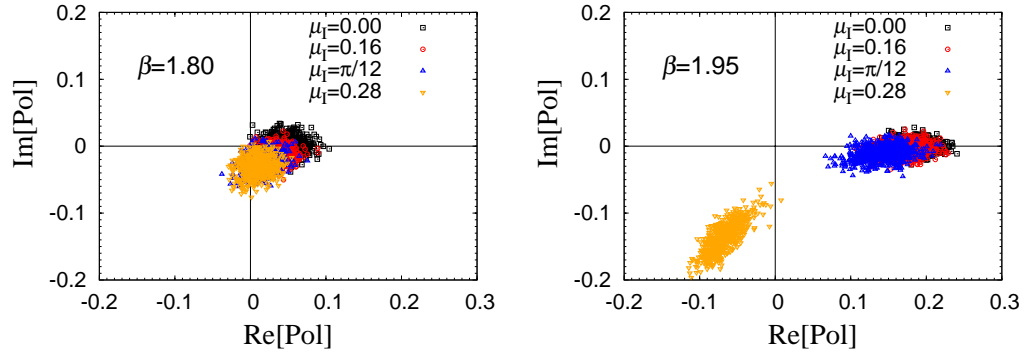


Figure 2: Scatter plots of the Polyakov loop. Left :  $\beta = 1.80$  (low temperature (below  $T_{pc}$ )). Right :  $\beta = 1.95$  (high temperature (above  $T_{RW}$ )).

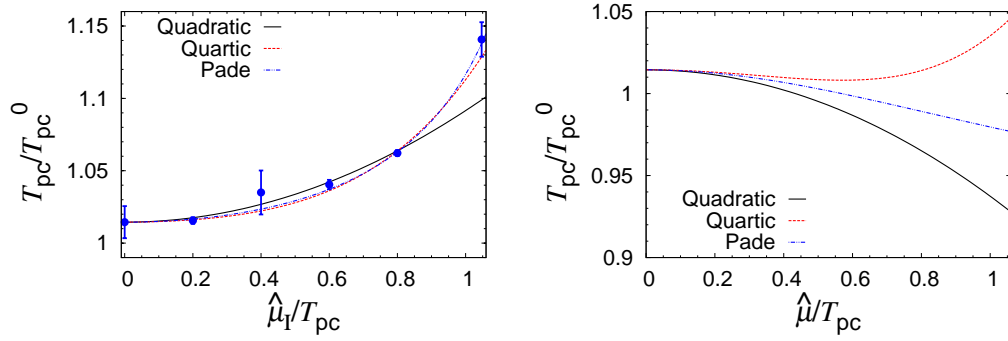


Figure 3: The pseudo-critical line  $\beta_{pc}$  in the imaginary (left panel) and real(right panel) region.

of the fermion determinant. In these approaches, the heaviest part of the numerical calculations is the evaluation of the determinant. An efficient way of the determinant evaluation is highly desirable. Here we introduce a matrix reduction formula for Wilson fermions, which was first constructed by Borici [21]. Later it was studied with the inclusion of the fugacity expansion [4, 22].

The Wilson fermion matrix defined in Eq. (2) can be divided into three terms according to their time dependence

$$\Delta = B - 2z^{-1}\kappa r_- V - 2z\kappa r_+ V^\dagger. \quad (2)$$

Here  $r_\pm = (r \pm \gamma_4)/2$  with the Wilson parameter  $r$  and  $z = e^{-\mu}$ . Each component is defined by

$$B(x, x') \equiv \delta_{x, x'} - \kappa \sum_{i=1}^3 \left\{ (r - \gamma_i) U_i(x) \delta_{x', x+\hat{i}} + (r + \gamma_i) U_i^\dagger(x') \delta_{x', x-\hat{i}} \right\} + S_{Clover}, \quad (3)$$

$$V(x, x') \equiv U_4(x) \delta_{x', x+\hat{4}}, \quad V^\dagger(x, x') \equiv U_4^\dagger(x') \delta_{x', x-\hat{4}}. \quad (4)$$

They satisfy  $VV^\dagger = I$ . Note that  $r_\pm$  are projection operators in the case that  $r = 1$ .

Now, we construct a reduction formula for the Wilson fermions. A starting point is to define a permutation matrix  $P = (c_a r_- + c_b r_+ V z^{-1})$  [21]. The parameters  $c_a$  and  $c_b$  are arbitrary scalar except for zero, and may be set to one. Since  $r_\pm$  are singular, the matrix  $P$  must contain both of them; otherwise  $P$  is singular. It is straightforward to check  $\det(P) = (c_a c_b z^{-1})^{N/2}$ , where  $N = 4N_c N_x N_y N_z N_t$ . Multiplied by  $P$ , the quark matrix is transformed into

$$\Delta P = (c_a B r_- - 2c_b \kappa r_+) + (c_b B r_+ - 2c_a \kappa r_-) V z^{-1}. \quad (5)$$

Carrying out the temporal part of the determinant, we obtain

$$\begin{aligned} \det \Delta P &= \begin{pmatrix} \alpha_1 & \beta_1 z^{-1} & & & \\ & \alpha_2 & \beta_2 z^{-1} & & \\ & & \alpha_3 & \ddots & \\ & & & \ddots & \beta_{N_t-1} z^{-1} \\ -\beta_{N_t} z^{-1} & & & & \alpha_{N_t} \end{pmatrix} \\ &= \left( \prod_{i=1}^{N_t} \det(\alpha_i) \right) \det(1 + z^{-N_t} Q), \end{aligned} \quad (6)$$

where  $Q = (\alpha_1^{-1} \beta_1) \cdots (\alpha_{N_t}^{-1} \beta_{N_t})$ , which is often referred to as a reduced matrix or transfer matrix. The block-

matrices  $\alpha$  and  $\beta$  are given by

$$\begin{aligned}\alpha_i &= \alpha^{ab,\mu\nu}(\vec{x}, \vec{y}, t_i) \\ &= c_a B^{ab,\mu\sigma}(\vec{x}, \vec{y}, t_i) r_-^{\sigma\nu} - 2c_b \kappa r_+^{\mu\nu} \delta^{ab} \delta(\vec{x} - \vec{y}),\end{aligned}\quad (7)$$

$$\begin{aligned}\beta_i &= \beta^{ab,\mu\nu}(\vec{x}, \vec{y}, t_i), \\ &= c_b B^{ac,\mu\sigma}(\vec{x}, \vec{y}, t_i) r_+^{\sigma\nu} U_4^{cb}(\vec{y}, t_i) - 2c_a \kappa r_-^{\mu\nu} \delta(\vec{x} - \vec{y}) U_4^{ab}(\vec{y}, t_i),\end{aligned}\quad (8)$$

where the dimensions of  $\alpha_i$  and  $\beta_i$  are given by  $N_{\text{red}} = N/N_t = 4N_x N_y N_z N_c$ . Substituting  $\det(P) = (c_a c_b z^{-1})^{N/2}$ , we obtain

$$\det \Delta = (c_a c_b)^{-N/2} z^{-N/2} \det \left( \prod_{i=1}^{N_t} \alpha_i \right) \det (z^{N_t} + Q). \quad (9)$$

Here,  $Q$  is independent of  $\mu$  and its rank is given by  $N_{\text{red}} = N/N_t$ , while that of the Wilson fermion is originally given by  $N$ .

With the eigenvalues  $\lambda_n = \{\lambda \mid \det(Q - \lambda I) = 0\}$ , the determinant of  $Q$  is given by

$$\det(z^{N_t} + Q) = \prod_{n=1}^{N_{\text{red}}} (\lambda_n + z^{N_t}). \quad (10)$$

Expanding this in powers of the fugacity  $z^{N_t} = e^{-\mu/T}$ , we finally obtain the reduced quark determinant

$$\det \Delta(\mu) = \sum_{n=-N_{\text{red}}/2}^{N_{\text{red}}/2} C_n (e^{\mu/T})^n, \quad (11)$$

Note that we redefine the index of  $c_n$  ( $c_n$  by  $c_{-n}$ ) to obtain the second line from the first one. Here,  $C_n = C c_n$  with  $C = (c_a c_b)^{-N/2} \left( \prod_{i=1}^{N_t} \det(\alpha_i) \right)$ .

Using a relation Eq. (1) and the reduction formula, one gets

$$(\xi^*)^{-\frac{N_{\text{red}}}{2}} \prod_{n=1}^{N_{\text{red}}} (\lambda_n^* + \xi^*) = (\xi^*)^{\frac{N_{\text{red}}}{2}} \prod_{n=1}^{N_{\text{red}}} (\lambda_n + (\xi^*)^{-1}), \quad (12)$$

where  $\xi = z^{N_t}$ . This holds for any  $\xi \in \mathbb{C}$ . For  $\xi = -\lambda_n$ , the left-hand side vanishes, and so should be the right-hand side. Then, the eigenvalue always appear in a set

$$\lambda_n, \quad 1/\lambda_n^* \quad (13)$$

The relation is also pointed out by Alexandru and Wenger [22].

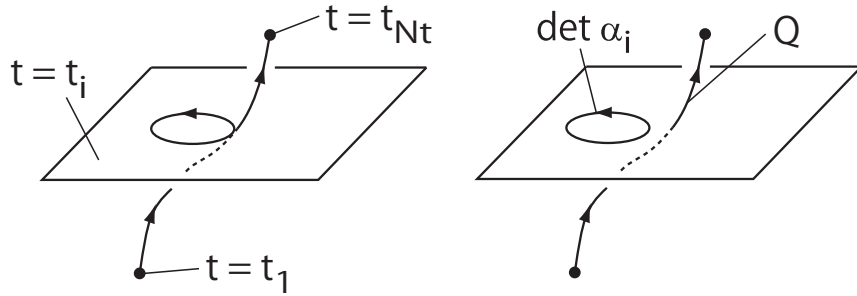


Figure 4: Schematic figures for the reduction procedure.

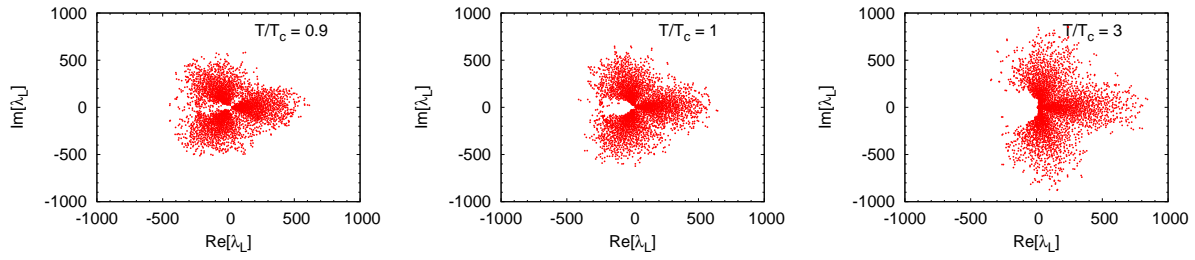


Figure 5: Distributions of the large eigenvalues in complex plane.

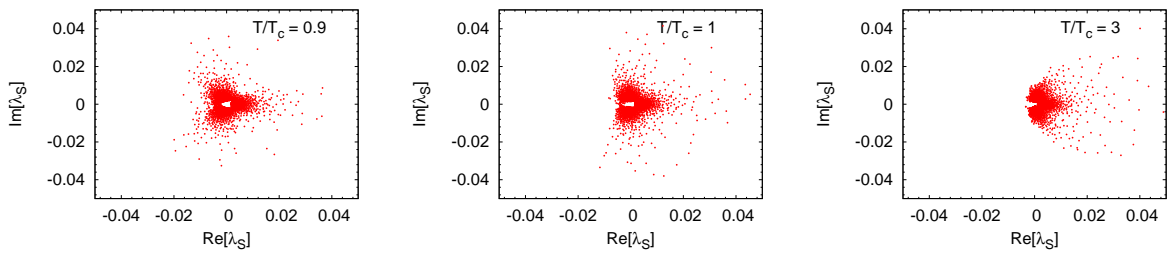


Figure 6: Distributions of the small eigenvalues in complex plane.

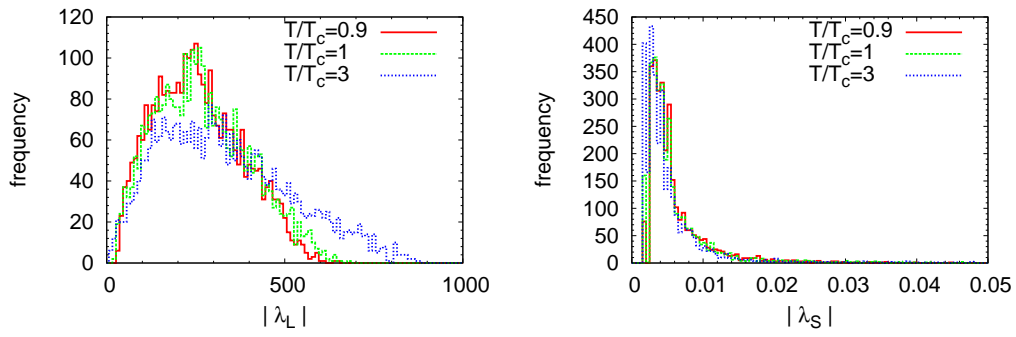


Figure 7: Histogram of the absolute value of  $\lambda$ . Left : large eigenvalues. Right : Small eigenvalue.

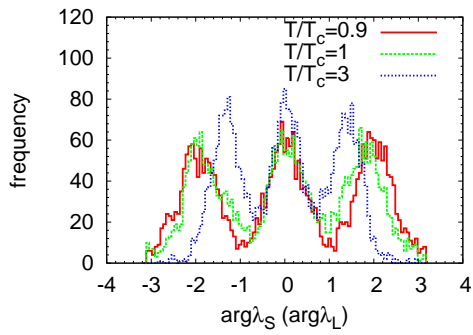


Figure 8: Histogram of the phase of  $\lambda$ .



The reduction formula makes it easier to calculate fermion determinant. We plan to evaluate the phase transition line at real chemical potential points. Combining estimations of the phase transition line both at real and chemical potential regions, we will get more reliable information about QCD phase structure.

Figures 5 and 6 show the scatter plot of  $\{\lambda\}$  for three different temperatures  $\beta = 1.80, 1.855, 2.0$ , which correspond to  $T/T_c = 0.9, 1, 1.3$ , respectively. Figures 7 and 8 show the histogram of the eigenvalue distribution. The simulation setup was the same as given in the previous section. Note that Fig. 6 enlarges a small domain near the origin in Fig. 5.

The eigenvalues are distributed in two separate regions, and there is a margin between the two regions, where no eigenvalue is found. The histogram of the absolute value of  $\lambda$  also show this behavior, see the right panel of Fig. 7.

The  $\beta$  dependence appears in the phase of  $\lambda$ ;  $\lambda$  are distributed in a  $Z_3$  symmetric manner at low temperatures, while not at high temperatures. The symmetric property is broken at high temperatures, and  $\lambda$  approach to real axis. Note that this behavior is observed both for small and large eigenvalues, because of the pair nature of  $\lambda$ .

The properties of the fugacity coefficients  $c_n$  was discussed in [4].

The simulation was performed on NEC SX-8R at RCNP, and NEC SX-9 at CMC, Osaka University, and HITACHI SR11000 and IBM Blue Gene/L at KEK. This work was supported by Grants-in-Aid for Scientific Research 20340055 and 20105003.

## References

- [1] A. Andronic *et al.*, Nucl.Phys. **A837**, 65 (2010), [0911.4806].
- [2] S. Muroya, A. Nakamura, C. Nonaka and T. Takaishi, Prog.Theor.Phys. **110**, 615 (2003), [hep-lat/0306031].
- [3] P. de Forcrand, PoS **LAT2009**, 010 (2009), [1005.0539].
- [4] K. Nagata and A. Nakamura, Phys.Rev. **D82**, 094027 (2010), [1009.2149].
- [5] K. Nagata and A. Nakamura, Phys.Rev. **D83**, 114507 (2011), [1104.2142].
- [6] A. Roberge and N. Weiss, Nucl. Phys. **B275**, 734 (1986).
- [7] P. de Forcrand and O. Philipsen, Nucl. Phys. **B642**, 290 (2002), [hep-lat/0205016].
- [8] M. D’Elia and F. Sanfilippo, Phys. Rev. **D80**, 111501 (2009), [0909.0254].
- [9] M. D’Elia and F. Sanfilippo, Phys.Rev. **D80**, 014502 (2009), [0904.1400].

- [10] P. de Forcrand and O. Philipsen, Phys.Rev.Lett. **105**, 152001 (2010), [1004.3144].
- [11] M. D’Elia and M.-P. Lombardo, Phys.Rev. **D67**, 014505 (2003), [hep-lat/0209146].
- [12] M. D’Elia and M. P. Lombardo, Phys.Rev. **D70**, 074509 (2004), [hep-lat/0406012].
- [13] M. D’Elia, F. Di Renzo and M. P. Lombardo, Phys.Rev. **D76**, 114509 (2007), [0705.3814].
- [14] P. Cea, L. Cosmai, M. D’Elia and A. Papa, Phys.Rev. **D81**, 094502 (2010), [1004.0184].
- [15] P. Cea, L. Cosmai, M. D’Elia, C. Manneschi and A. Papa, Phys.Rev. **D80**, 034501 (2009), [0905.1292].
- [16] P. Cea, L. Cosmai, M. D’Elia and A. Papa, Phys.Rev. **D77**, 051501 (2008), [0712.3755].
- [17] L.-K. Wu, X.-Q. Luo and H.-S. Chen, Phys. Rev. **D76**, 034505 (2007), [hep-lat/0611035].
- [18] WHOT-QCD Collaboration, S. Ejiri *et al.*, Phys.Rev. **D82**, 014508 (2010), [0909.2121].
- [19] O. Philipsen, Prog.Theor.Phys.Suppl. **174**, 206 (2008), [0808.0672].
- [20] A. Gocksch, Phys.Rev.Lett. **61**, 2054 (1988).
- [21] A. Borici, Prog. Theor. Phys. Suppl. **153**, 335 (2004).
- [22] A. Alexandru and U. Wenger, Phys.Rev. **D83**, 034502 (2011), [1009.2197].